PCCP

Accepted Manuscript

ROYAL SOCIETY OF CHEMISTRY

www.rsc.org/pccp

PCCP

RSCPublishing

ARTICLE

Polymer Nanofibers: Preserving nanomorphology in ternary blend organic photovoltaics†

Cite this: DOI: 10.1039/x0xx00000x

Received ooth January 2012,
Accepted ooth January 2012

DOI: 10.1039/x0xx00000x

www.rsc.org/

Teddy Salim,[a] Jun Yan Lek,[a] Björn Bräuer,[b] Denis Fichou[c,d,e] and Yeng Ming Lam*[a]

The morphology of donor-acceptor blends holds the key to good performance through the balancing of good exciton dissociation efficiency and interconnectivity for good charge collection. In this work, the good morphology is preserved in ternary blend system through the use of poly(3-hexylthiophene) (P3HT) nanofibers. Iridium(III)-based metal complex is incorporated in P3HT-PCBM blend as triplet exciton sensitizer on the bulk heterojunction (BHJ) organic photovoltaics (OPV). The devices using triplet-sensitized ternary blends of P3HT experience a significant degradation in performance, a tendency further aggravated by thermal treatment. This is due to disruption in the morphology thus affecting charge generation and collection. In order to overcome these morphological issues and to circumvent the restriction due to the crystallization of the polymers, here we demonstrate the use of pre-assembled nanofibers in these ternary blends. The concept of stabilizing the nanomorphology of the blend material through the use of nanofibers can also be applied to other ternary systems.

1. Introduction

The field of organic photovoltaics (OPV) has become progressively more attractive in recent decade and is regarded as one of the most promising emerging technologies for renewable energy industry. It offers a viable alternative for large-scale manufacturing of lightweight flexible photovoltaic devices through low-cost solution processing.[1-4] In addition, the chemical and optoelectronic properties of the components used in OPV can be easily tailored by means of various synthetic chemistry techniques.[5, 6] The current state-of-the-art in OPV technology adopts the concept of the bulk heterojunction (BHJ), in which a *p*-type donor (D) material is blended with an *n*-type acceptor (A) to form the photoactive layer sandwiched between electrodes with different work functions. Significant improvement in power conversion efficiencies (PCE) of BHJ-based OPV devices in excess of 9% and 10% have been demonstrated for polymer–fullerene blends with single-junction and tandem architecture, respectively.[7, 8] These high PCEs can only be obtained when both D and A form an optimal morphology with interpenetrating nanoscale networks favorable for both exciton dissociation and charge transport.[9] Various techniques such as thermal annealing,[10] solvent annealing,[11] solvent additive[12-14] and application of preformed polymer nanostructures,[15-17] have been applied to BHJ blends to induce a more thermodynamically stable and optimally phase-separated blend morphology. Among the strategies pursued to boost the performance of BHJ-based OPV devices are engineering of device interfaces,[18-21] employing tandem architectures,[22, 23] and introducing dopant materials into the binary blends to generate ternary systems.[24-33] Ternary blend serves as a simple yet effective method to improve device performance through the incorporation of dopant materials with superior optical and electrical properties into the existing mixtures. Another type of the dopants often used in the ternary systems is triplet material, *e.g.* organometallic compounds.[31-33]

The concept of triplet exciton was first introduced as a prospective panacea for the issue of short exciton diffusion length (L_D) universal in OPV devices.[34] Due to the low degree of order in OPV materials, L_D is typically on the order of 5–20 nm for singlet excitons.[35] In order to allow efficient dissociation of these excitons, the thickness of the active layer has to be within L_D. Unfortunately a thickness (d) of ≥100 nm is required to ensure maximum absorption of the incident photons. Increasing the lifetime of excitons, which can in turn increase L_D, increases the probability of exciton-to-carrier conversion before they decay. Since radiative decay of triplet excitons is dipole-forbidden, their lifetime is typically longer (μs to ms) as compared to that of singlet excitons (ns) rendering them attractive as a potential solution to the L_D vs d dilemma. This issue can also be overcome by using the bulk heterojunction (BHJ) concept, which requires the domain size be smaller than

twice the diffusion length; with the presence of more triplet excitons, the tolerable domain size becomes even greater.

Although the efficacy of the triplet exciton-enhanced OPV remains controversial, research in the field has shown a few encouraging results leading to an increasing number of publications in recent years. Strengthening the spin-orbital coupling of organic systems can be done through introduction of transition metals into OPV systems (*e.g.* iridium, platinum, or palladium complexes) which act as platforms for singlet states to intersystem cross to form triplet states.[36] These metal complexes can be either chemically tethered to the backbones of conjugated polymers[37-41] or physically dispersed in the donor-acceptor BHJ.[31-33] Recently, it was also demonstrated that singlet-to-triplet conversion could be enhanced by adding spin ½ radicals, *e.g.* galvinoxyl.[42] Triplet OPV has also been successfully applied in planar double heterojunction configuration, in which the complexes are only mixed with either one of the active materials, usually the donors.[43-46] A major problem with the incorporation of a third component in a binary system is that the dopant can have counter-productive effects on the blend morphology and consequently annihilate the expected advantages. Both exciton dissociation and charge transport could be adversely affected in a blend with poor morphology. In fact in a recent report by Rao *et al.*, the recombination of the triplet states can be suppressed in organic polymer/fullerene-based BHJ system if the films have high degree of crystallinity in the fullerene phase compared to a system with higher disorder.[47] Hence film morphology is even more critical in a system that involves triplet sensitization. This is confirmed by another theoretical work by Bittner *et al.* where they found that the decay of the triplet states in these systems is enhanced by energetic disorder.[48] There is a fine balance in the degree of order in such blend films.

In this work, we investigate the influence of nanomorphology of ternary blends of poly(3-hexylthiophene-2,5-diyl):[6,6]-phenyl-C_{61}-butyric acid methyl ester (P3HT:PCBM) mixed with iridium tris(2-phenylpyridine) ($Ir(ppy)_3$) as triplet sensitizers. In particular we compare blends of P3HT with and without nanofibers (NF). Both types of devices were prepared based on their own optimized fabrication conditions. The P3HT:PCBM blend device shows a decrease in performance with the inclusion of iridum complex due to the disruption of its optimal morphology. The phase aggregation becomes too severe with thermal annealing. To reduce the detrimental effect on the morphology, highly organized pre-assembled P3HT nanofibers were prepared and used in the ternary blends. We could observe a triplet sensitization effect in the P3HT-NF:PCBM system, showing that it is possible to circumvent the limitation caused by thermal annealing. This emphasizes the importance of polymer nanostructures in small molecule-doped ternary composites and opens the way to new strategies in the design of efficient OPV materials.

2. Experimental details

Materials

Regioregular poly(3-hexylthiophene-2,5-diyl) P3HT (M_W = 48.3 kDa, regioregularity > 90%) was purchased from Rieke Metals, Inc., while [6,6]-phenyl-C_{61}-butyric acid methyl ester (PCBM) (99.5% purity) was obtained from Nano-C®. The triplet metal complex, *fac*-tris(2-phenyl-pyridinato-C^2,*N*)iridium(III) ($Ir(ppy)_3$) (99% purity), solvents 1,2-dichlorobenzene (*o*-DCB) (Chromasolv® HPLC grade, 99%) and *p*-xylene were purchased from Sigma Aldrich. Poly(3,4-ethylenedioxy-thiophene):poly-(styrenesulfonate) (PEDOT:PSS) (P VP Al 4083) was purchased from CLEVIOS™. All chemicals were used as received without further purification.

Nanofiber solution preparation

P3HT nanofiber (P3HT-NF) solution was prepared by slow cooling of dissolved P3HT solution (7 mg/mL) in *p*-xylene from 85 °C at the rate of 10 °C/h using refrigerated circulator (Julabo F25-EC). After being gradually cooled to room temperature, the solution was then left undisturbed in dark for the next 48 h to ensure sufficient nanofiber formation before being mixed with PCBM.

Device fabrication and measurement

The blend solutions were prepared by mixing P3HT (10 mg/mL) with PCBM in *o*-DCB with weight ratio of 10:10. To prepare the ternary blend solutions, 5 wt% of $Ir(ppy)_3$ was added into the previously prepared binary blends of P3HT:PCBM (P3HT:PCBM:$Ir(ppy)_3$ = 10:10:1). The D:A ratio for the P3HT-NF blend was 10:6, and the $Ir(ppy)_3$ amount was adjusted accordingly. The mixtures were stirred overnight at 50 °C in N_2 atmosphere, while the nanofiber blend was stirred at room temperature. The devices were prepared on indium-tin oxide (ITO) coated glass substrates (7 Ω/sq, Kintec Company). The substrates were consecutively ultrasonicated in cleaning concentrate (Hellmanex®), deionized water, acetone and isopropanol. After the substrates were dried under a stream of N_2, they were plasma cleaned for 2 min (Harrick PDC-32G plasma cleaner). Subsequently, PEDOT:PSS solution was filtered through 0.45 μm PVDF syringe filter and spin-coated onto the ITO-coated glass substrates at 3000 rpm for 60 s to give films of *ca.* 30 nm thickness. The PEDOT:PSS coated substrates were transferred into a N_2 glovebox and were baked on a hotplate at 140 °C for 10 min. The active layers were then deposited by spin-coating the blend solutions to give films with thicknesses of 90 ± 10 nm. To complete the device fabrication, *ca.* 100 nm of Al was deposited onto the samples in vacuum (< 10^{-6} Torr) resulting in devices with an active area of 0.1 cm^2. The P3HT-based binary and ternary devices were subjected to further post-deposition thermal annealing under N_2 at 150 °C for 20 min. No thermal annealing was performed on nanofiber devices. The electrical properties of the OPVs were characterized by measuring their current density-voltage (*J*-V) characteristics in ambient under AM 1.5G illumination with a

sourcemeter (Keithley 2400). The light intensity was adjusted to 1 sun (100 mW/cm^2) with an NREL-calibrated silicon photodiode. The obtained *J*-V characteristics were not corrected with mismatch factor. External quantum efficiency (EQE) measurement was done with a Merlin radiometer (Newport) under monochromatic illumination. A calibrated Si photodiode was used as reference device in counting incident photons.

Blend Characterizations

The UV-Visible absorption spectra of the blend films prepared on quartz substrates were characterized using Shimadzu UV-2510PC spectrometer. The film thickness was measured with a surface profilometer (Alpha Step 200, KLA-Tencor™). Atomic force microscopy (AFM) was done in tapping mode on the active layers of the devices with a surface probe microscope (Digital Instruments, Nanoscope IIIa). The obtained images were processed with WSxM 5.0 (Nanotec Electronica). Grazing incidence X-ray diffraction (GIXRD) was performed with θ/θ geometry (Bruker D8 Discover) and a Göbel mirror was used. The parallel X-ray beam allows grazing incidence diffraction due to its low divergence, in addition to an enhancement of the X-ray beam intensity. Cu Kα1 radiation at 1.54056 Å was used together with 1-D detector. The grazing incidence angled was 0.7o. Near edge X-ray absorption fine structure (NEXAFS) spectroscopy and scanning transmission X-ray microscopy (STXM) were performed at the elliptical polarizing undulator (EPU) beamline 11.0.2 at the Advanced Light Source in Berkeley, California (USA). Photon energies of 280 eV, 284.8 eV and 286.2 eV were used for the STXM imaging. For both NEXAFS and STXM studies, the samples were prepared by spin-coating the active material/ blend solutions on silicon nitride membranes. All measurements were done at room temperature in He atmosphere. Each image was taken within 5 to 8 min, which means that one molecule is exposed to X-rays for less than 10 ms. The radiation damage is negligibly low and does not influence the experimental results.

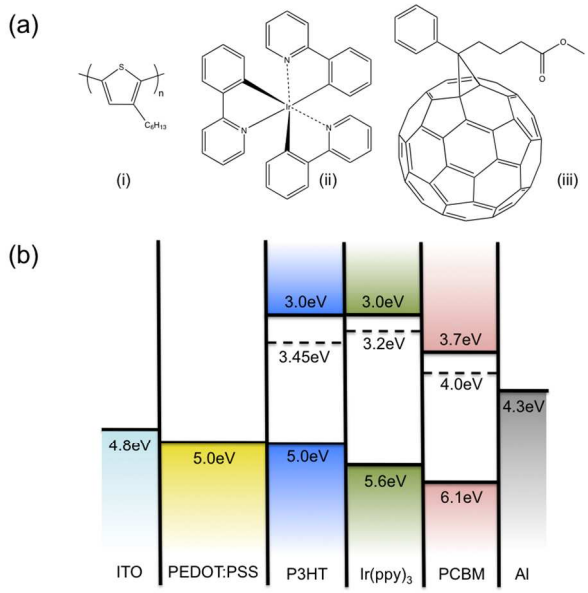

Fig. 1 (a) Chemical structures of the ternary blend components: (i) P3HT, (ii) Ir(ppy)$_3$ and (iii) PCBM. (b) Energy level diagram of the components in the ternary blend devices. The dotted lines represent the triplet energy levels (with respect to the HOMO levels).

3. Results and discussion

Energy levels

Fig. 1b shows the electronic energy diagram of the active components in the ternary blend. The solid lines represent the molecular orbital energy levels (HOMOs and LUMOs) while the dotted ones represent the estimated triplet energy levels. The molecular orbital energy level values shown were extracted from established literatures, with justified approximation.[49-51] The triplet levels for both P3HTs were estimated based on the exchange energy between the lowest singlet state and the triplet state (ΔE_{ST}), which was found to hold a value of *ca.* 0.7 eV for various amorphous π–conjugated polymers[52] and *ca.* 0.45 eV for ordered poly(3-alkylthiophene).[53] The triplet energy level for Ir(ppy)$_3$ was derived from its phosphorescence peak.[51] The LUMO level, or lowest excited singlet state (S_1), of P3HT is similar to that of Ir(ppy)$_3$ (*ca.* 3 eV) suggesting that upon excitation singlet excitons in the donor P3HT may readily delocalize between the two materials, followed by rapid intersystem crossing (ISC) to the triplet state (T_1) in the triplet dopant. Furthermore, the triplet excitons in Ir(ppy)$_3$ may either back-transfer and populate T_1 of P3HT or get quenched *via* electron transfer to S_1 of PCBM. Due to the rapid (picoseconds range) photoelectron transfer to PCBM, the latter is the kinetically more preferred process.[37] Following the charge transfer, intersystem crossing from S_1 to T_1 states in PCBM is also possible depending on the energy of the charge-separated state.[54] The HOMO level of Ir(ppy)$_3$, which is between those of P3HT and PCBM, not only prevents hole trapping in the dopant material, but also allows hole transfer between donor and acceptor. To sum up, the introduction of iridium-based dopant does not pose any energetic barrier to the photoinduced charge generation. Nevertheless, the physical distance between the triplet and the donor molecules has to be kept minimal to ensure efficient triplet sensitization. This limitation is closely related to the issue of the optimal blend morphologies, which will be discussed later.

Optical characteristics

Fig. 2 shows the solid-state UV-Vis absorption spectra of both P3HT:PCBM and P3HT-NF:PCBM (before and after addition of the triplet dopant, Ir(ppy)$_3$). The nanofiber blends exhibit more pronounced vibronic "shoulders" at *ca.* 560 nm and *ca.* 620 nm, which indicates high degree of order. The inset shows that Ir(ppy)$_3$ absorbs throughout the visible spectrum, even extending to the UV region with a peak absorption at 390 nm. Incorporation of the Ir(ppy)$_3$ molecules does not affect the absorption characteristics of P3HT, as seen from the nearly

overlapping profiles. The triplet dopant (5 wt%) slightly increases the absorption of both blends around 340–450 nm regardless of the nanofiber presence. The effect of the presence of triplet dopant on the ordering of the blend materials is discussed in the following GIXRD section.

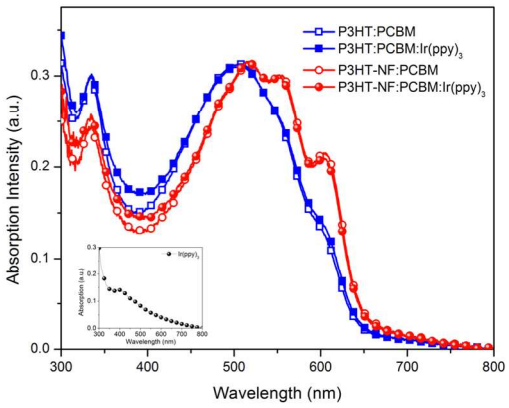

Fig. 2 UV-Vis absorption spectra of P3HT:PCBM and P3HT-NF:PCBM blends, with and without $Ir(ppy)_3$ incorporation. The P3HT:PCBM films were thermally annealed at 150 °C for 20 min. The samples were prepared on quartz substrates. The inset shows UV-Vis absorption characteristics of $Ir(ppy)_3$ in solid state.

Structural and morphological characteristics

Fig. 3 shows the GIXRD spectra for both non-fiber and nanofiber blend systems. The nanofiber samples show first, second and even third order reflections indicating the presence of reasonably long-range order. This corresponds well to the previous absorption data. The blend films without nanofibers only show first and second order peaks indicating ordering in P3HT molecules but to a lesser extent compared to the nanofiber films. In the presence of $Ir(ppy)_3$, the organization of P3HT is not disrupted. The diffraction peak at 2θ = 10.8° corresponds to (200) planes of the $Ir(ppy)_3$ crystals.[55] This peak overlaps with the second order peak of P3HT in P3HT-NF:PCBM:$Ir(ppy)_3$ film. On the other hand, the organization of PCBM is not obvious from the GIXRD spectra except for the spectra of the samples containing $Ir(ppy)_3$ that show a peak at 2θ = 16.7° corresponding to some ordering in PCBM phase.

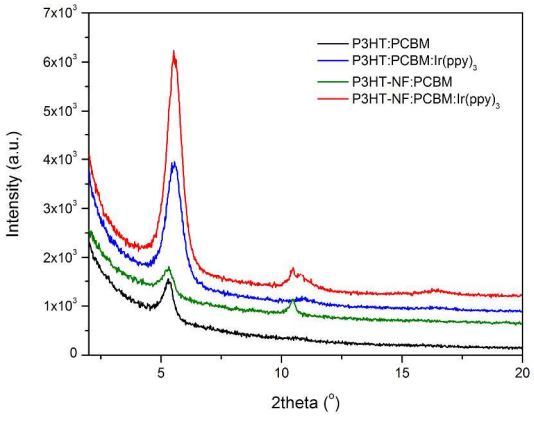

Fig. 3 GIXRD patterns of P3HT:PCBM and P3HT-NF:PCBM, with and without $Ir(ppy)_3$ incorporation. The P3HT:PCBM films were thermally annealed at 150 °C for 20 min. The samples were prepared on Si substrates.

Variation in blend morphology has significant effects on the device performances. It was observed that $Ir(ppy)_3$ tends to form one-dimensional nanostructures in polymer composites, as evident from the needle-like features (length of 1–5 μm, width of *0.6–1.2* μm and aspect ratio of *ca.* 8) present throughout the P3HT surface (Fig. S1). Wang *et al.* also reported the formation of similar structures by a gradual solvent evaporation technique.[55] Our observation is suggestive of the ability of $Ir(ppy)_3$ molecules to self-assemble into nanostructures even under rapid solvent evaporation condition such as spin-coating. Further blending with PCBM obviously does not disrupt the formation of those nanostructures (Fig. 4d). The high amount of PCBM in the ternary blends (*i.e.* ten times higher than $Ir(ppy)_3$) may have interfered in the self-assembly of $Ir(ppy)_3$ molecules, thus resulting in the reduction of the needle lengths (<1–3 μm)

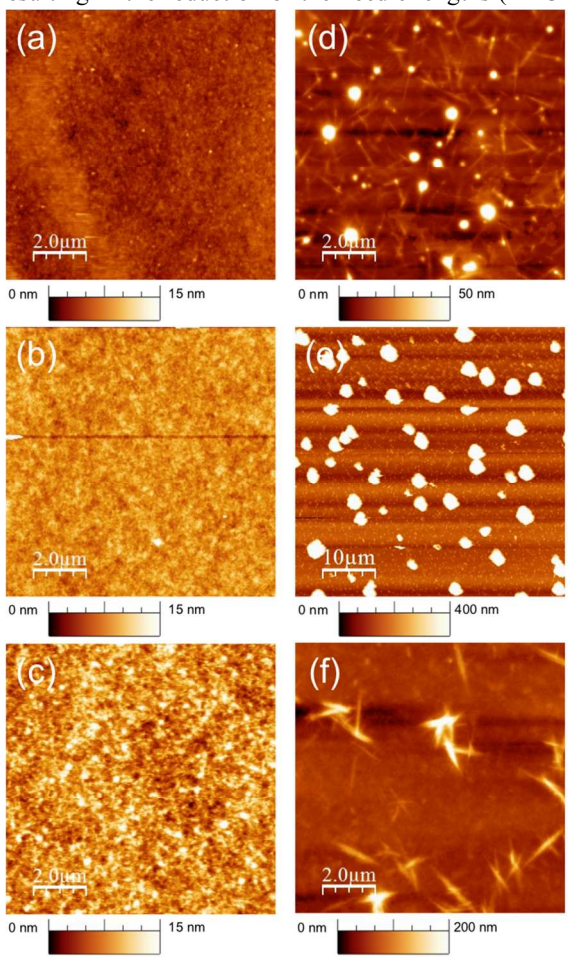

Fig. 4 Tapping mode AFM height images of: (a,d) as-cast P3HT:PCBM, (b,e) thermally annealed P3HT:PCBM and (c,f) P3HT-NF:PCBM. Thermal annealing was done at 150 °C for 20 min. The left images (a–c) correspond to the binary blends; the right images (d–f) correspond to the ternary blends with $Ir(ppy)_3$ incorporation.

and smaller width (80–100 nm) with a significantly increased aspect ratio (*ca.* 10–40). Similar phenomenon was also seen in P3HT-NF:PCBM blend with $Ir(ppy)_3$ additive (Fig. 4f). It is noticeable that the needle coverage is much less than in the nonfiber blend, although the needles are similar in dimension (*ca.* 1–3 μm in length). This suggests that $Ir(ppy)_3$ molecules are better distributed in the bulk of the nanofiber blend, and are thus more likely to sensitize the active materials. The formation of the iridium needles, however, was not observed in the heat-treated P3HT:PCBM sample.

P3HT readily undergoes local molecular packing, which becomes more pronounced upon thermal treatment. Thermal annealing beyond glass transition temperatures (T_g) of the materials magnifies the extent of molecular phase segregation in P3HT blends since the strong crystallization of the polymer phase will in turn provide a large free volume for the small molecules such as $Ir(ppy)_3$ to interact with and thus coalesce into larger aggregates. As a result, large cube-like particles with diameter of *ca.* 1–3 μm and height of > 1 μm emerge on the surface of the heat-treated P3HT:PCBM:$Ir(ppy)_3$ film (Fig. 4e). These particles (also seen in Fig. S2) are most likely hybrid structures of both triplet dopants and fullerene molecules. Upon annealing, PCBM molecules tend to form needle-like crystals with lengths of *ca.* 100 μm instead of micron-sized cuboids. Moreover, a separate annealing study of P3HT:$Ir(ppy)_3$ (without PCBM) did not induce any significant morphological change either. Nevertheless, in the triplet-doped blends, thermal annealing resulted in the formation of large cube-like particles, suggesting that the presence of the triplet dopants triggered their emergence. This also suggests that PCBM molecules may have diffused and nucleated on the surfaces of $Ir(ppy)_3$ crystals. This type of heterogeneous nucleation and growth may have resulted in $Ir(ppy)_3$/PCBM core/shell hybrid nanostructures. The co-existence of both PCBM and $Ir(ppy)_3$ molecules in the cube-like particles is further elucidated *via* scanning transmission X-Ray microscopy (STXM) study.

Based on the near edge X-ray absorption fine structure (NEXAFS) spectra (Fig. 5a), photon energies of 284.8 eV and 286.2 eV were used, corresponding to the absorption peaks of $Ir(ppy)_3$ and PCBM, respectively. The difference in the X-ray absorption intensity between $Ir(ppy)_3$ and PCBM at 284.8 eV is marginal, while the absorption intensity of PCBM is much higher for 286.2 eV. Fig. 5b shows the X-ray microscopy images of thermally annealed ternary blends of P3HT:PCBM:$Ir(ppy)_3$ taken at both photon energies. The emergence of the micron-sized particles with high contrast is in good accordance with the previous AFM results (Fig. 4e). These particles absorb strongly at 284.8 eV and 286.2 eV, which indicates that they contain both $Ir(ppy)_3$ and PCBM. At 286.2 eV (PCBM absorption), these micron-sized particles appear to be darker suggesting that they are rich in PCBM (Figure 5b(ii)). Thermal treatment should have induced the aggregation of PCBM molecules on iridium crystals to form the large aggregates, which may have detrimental effects on device performance.

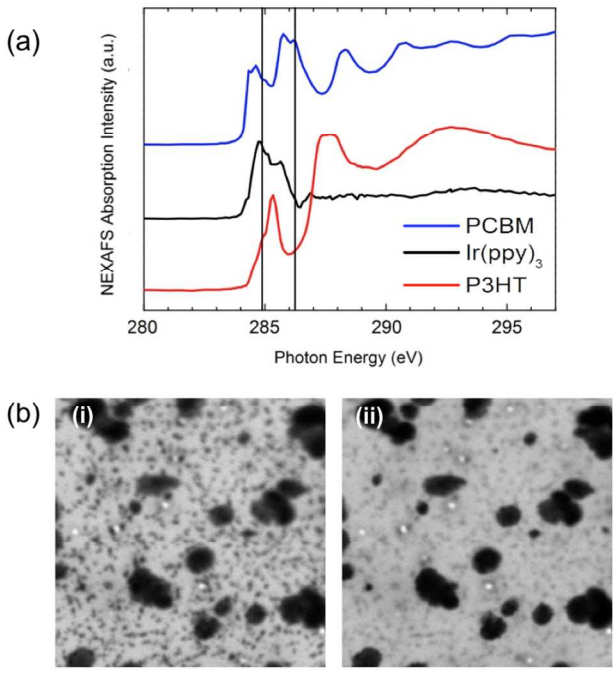

Fig. 5 (a) NEXAFS spectra of P3HT, PCBM and $Ir(ppy)_3$. The vertical lines indicate the photon energies used for STXM imaging (284.8 eV and 286.2 eV corresponding to $Ir(ppy)_3$ and PCBM absorption peaks, respectively). (b) STXM images for P3HT:PCBM:$Ir(ppy)_3$ ternary blend, thermally annealed at 150 °C for 20 min. The left image was taken at 284.8 eV; the right image was taken at 286.2 eV.

Device characteristics

The morphological effects of the triplet sensitizer on the binary blends will inadvertently influence the performance of the photovoltaic devices fabricated using these films. Fig. 6a displays the current density-voltage (*J*–V) characteristics of the devices under AM1.5G illumination (100 mW/cm^2). The device performance data is provided in Table 1. The heat-treated binary device of P3HT:PCBM exhibits power conversion efficiency (PCE) of 2.96% with short-circuit current (J_{SC}) of 9.02 mA/cm^2, open-circuit voltage (V_{OC}) of 0.57 V and fill factor (FF) of 0.57. The thermally activated diffusion of both P3HT and PCBM molecules results in a higher PCE that the as-cast device due to the enhanced molecular reorganization with increased degree of crystallinity for both materials.[56] The incorporation of $Ir(ppy)_3$ molecules into the P3HT:PCBM blend further degrades device PCE to 0.81% (> 70% reduction), due to decrease in J_{SC}, FF and even V_{OC}. The considerably reduced V_{OC} from 0.58 to 0.43 V in the TA P3HT:PCBM:$Ir(ppy)_3$ may be attributable to substantial PCBM aggregation.[14] The decrease in both J_{SC} and FF also indicates poorer charge transport with increased series resistance (bulk and contact resistances) caused by the presence of the particles that result from a more extreme aggregation. Although some ordering is beneficial for triplet recombination kinetics, this advantage is offset by its adverse effects on the electrical transport properties in the film.[47]

Semicrystalline polymers (such as P3HT) tend to be superior in terms of their electronic properties as compared to amorphous polymers. However, their molecular miscibility with small molecules, either acceptors or dopants, may become an issue due to their propensity to interact among themselves and self-organize. The phase separation is aggravated upon thermal treatment. Unfortunately thermal annealing is necessary in order to achieve excellent electronic properties for P3HT-PCBM blends. Furthermore, the presence of a third component in the system, to a large extent, may also affect the blend morphology. As discussed above, thermal annealing of P3HT:PCBM:Ir(ppy)$_3$ generates microstructures which have a negative impact on device characteristics. However, by using polymer nanofiber approach, it is possible to obtain highly efficient solar cell devices without undergoing any post-fabrication annealing. The P3HT nanofibers (P3HT-NF) can be pre-formed in solution phase, with typical dimensions of a few microns in length and a few tens of nanometers in width (Fig. S3). Therefore, by eliminating the detrimental heat treatment step, ternary blends containing P3HT-NF may show triplet sensitization effect and hence improved device performance.

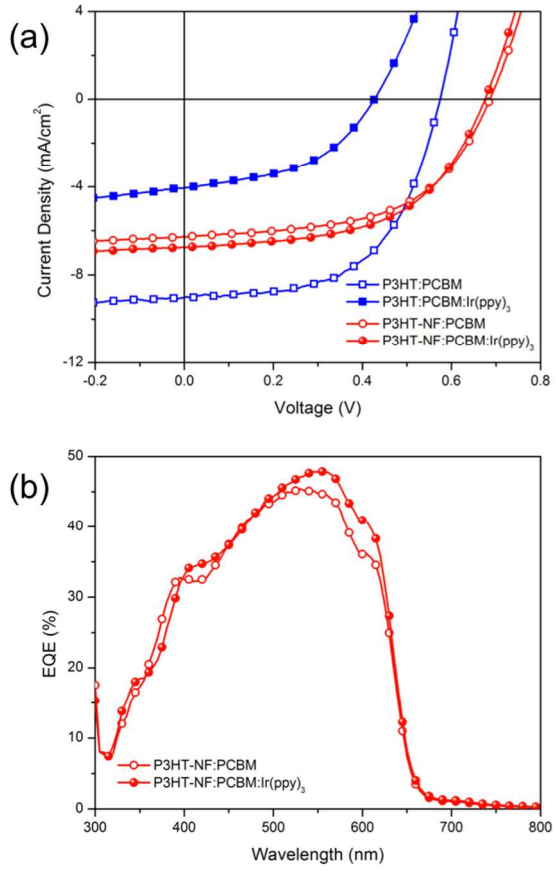

Fig. 6 (a) *J*-V characteristics of P3HT:PCBM and P3HT-NF:PCBM devices, with and without Ir(ppy)$_3$ incorporation. The P3HT:PCBM devices were thermally annealed at 150 °C for 20 min, while P3HT-NF:PCBM devices were not annealed. (b) EQE spectra of P3HT-NF:PCBM devices, with and without Ir(ppy)$_3$ incorporation.

Table 1 Summary of device parameters of various P3HT:PCBM devices.

Sample	PCE (%)	J_{SC} (mA/cm^2)	V_{OC} (V)	FF
P3HT:PCBM	2.96	9.02	0.57	0.57
P3HT:PCBM:Ir(ppy)$_3$	0.81	4.06	0.42	0.47
P3HT-NF:PCBM	2.37	6.30	0.68	0.55
P3HT-NF:PCBM:Ir(ppy)$_3$	2.49	6.75	0.67	0.55

The control P3HT-NF:PCBM binary device shows J_{SC} of 6.3 mA/cm^2, V_{OC} of 0.684 V, FF of 0.55 and PCE of 2.37%. On the other hand, the triplet-doped device shows J_{SC} of 6.75 mA/cm^2, V_{OC} of 0.673 V, FF of 0.55 and PCE of 2.49%. There is a slight improvement in the photocurrent by *ca.* 6% while the FF remains the same. These results show a noticeable difference from the previous data of the non-fiber P3HT:PCBM devices. The nanofiber device not only does not deteriorate in performance, but also shows a slight increase in PCE of *ca.* 5% upon Ir(ppy)$_3$ incorporation. The PCE increase is solely due to the improvement in J_{SC}, implying the possibility of an enhancement in the triplet excitons as induced by the intersystem crossing (ISC) process. This is aided by the fact that the recombination decay of these triplet states is reduced by the ordering in the fullerene phase as a result of the heterogeneous nucleation of ordered PCBM on the Ir(ppy)$_3$ molecules. The energetic disorder in the fullerene phase has an impact on the decay of these states, as discussed by Bittner *et al.*[48] The unaltered FF also indicates that Ir(ppy)$_3$ does not increase the device resistance. In addition, there is a more thorough device optimization by incorporating triplet molecules needs to be pursued in the future.

To understand the origin of the photocurrent (J_{SC}) enhancement observed in the nanofiber system, we performed external quantum efficiency (EQE) measurement (Fig. 6b). There is an apparent increase in the maximum EQE from 45% to 48% after the incorporation of the iridium complexes. The EQE enhancement in P3HT-NF:PCBM is observed to come from two main regions, *i.e.* around 420 nm and 500–620 nm. Rand *et al.* proposed multiple roles a triplet dopant may assume in the photocurrent generation in an OPV: (1) increasing triplet population in the donor material *via* sensitized phosphorescence, (2) directly absorbing photons followed by charge transfer to the nearby acceptor molecules, and (3) acting as auxiliary donor sites to help exciton dissociation from the acceptor molecules.[32] The increase in the EQE signal indicates that the Ir(ppy)$_3$ molecules fulfilled the first two roles. The improved absorption around 420 nm (Fig. 2), which corresponds to the absorption maximum of the iridium complex, suggests that the triplet molecules may have assisted the current generation through direct photoabsorption. On the other hand, the signal enhancement at 500–620 nm implies a selective triplet sensitization of the P3HT nanofibers. The data suggests that the triplet complexes must be distributed in close proximity to the polymer nanofibers.

Here we need to emphasize although the triplet-sensitized P3HT:PCBM device still underperforms the heat-treated P3HT-NF:PCBM device, it successfully demonstrates the benefit of

triplet sensitization. The triplet concept can also be extended to various low bandgap polymer systems. Advanced organometallic synthetic approaches also enable fine-tuning of the dopant energy levels to match those of the polymers. Besides, the versatility of organic synthesis techniques also enables the incorporation of a range of functional groups into the metal complexes, which can then be used to moderate molecular aggregation via steric control and T_g adjustment. When it is mandatory to organize the polymer molecules, there is an option to transform the polymers into well-defined nanostructures rather than to put them at the risk of heat-induced morphological damages. Although the triplet sensitization of the nanofiber device presented here is yet to be fully optimized, it is obvious that the approach is very promising when severe morphological issues occur upon dopant incorporation.

4. Conclusions

This study has clearly revealed that the morphology of ternary polymer–fullerene–dopant blends plays a significant role in the photovoltaic performances. Upon addition of iridium metal complex $Ir(ppy)_3$ into the P3HT:PCBM blend, a noticeable degradation in the device characteristics was observed. The metal complex essentially acts as a heterogeneous nucleus for the PCBM aggregates to form. Pre-formed nanostructure such as nanofiber is less likely to be affected by the third component in the system. Triplet sensitization could then be observed in the P3HT nanofiber (P3HT-NF) device. In such system, the detrimental thermal annealing step can be avoided without compromising the superior optoelectronic properties of P3HT. As a result, J_{SC} improves in the triplet-doped P3HT-NF:PCBM devices.

The concept of ternary blends opens up the possibility of enhancing the performances of simple bulk heterojunction (BHJ) devices through the incorporation of an optoelectronically compatible material. As shown here, in order to obtain this enhancement, the issues pertaining to the chemical nature of the polymer and morphology of the blend need to be carefully assessed and overcome. We are presently extending the ternary approach to other types of donor systems, in particular the low bandgap polymers.

Acknowledgements

The Advanced Light Source is supported by the Director, Office of Science, and Office of Basic Energy Sciences of the U.S. Department of Energy under Contract No. DE-AC02-05CH11231. B.B. thanks the Funds of Chemical Industry (Liebig Scholarship) for the financial support. We thank Assoc. Prof. Andrew C. Grimsdale (MSE/NTU) for his most helpful comments on our manuscript.

Notes and references

[a] *School of Materials Science and Engineering, Nanyang Technological University, 50 Nanyang Avenue, Singapore, 639798, Singapore. Tel: +65 6790 4260; E-mail: ymlam@ntu.edu.sg*
[b] *Stanford Institute for Materials and Energy Science, Stanford University, CA, 94025, USA.*
[c] *Sorbonne Universités, UPMC Univ Paris 06, UMR 8232, Institut Parisien de Chimie Moléculaire, F-75005, Paris, France*
[d] *CNRS, UMR 8232, Institut Parisien de Chimie Moléculaire, F-75005, Paris, France.*
[e] *School of Physical and Mathematical Sciences, Nanyang Technological University, Singapore 637371.*

† Electronic Supplementary Information (ESI) available: [details of any supplementary information available should be included here]. See DOI: 10.1039/b000000x/

1. C. J. Brabec, S. Gowrisanker, J. J. M. Halls, D. Laird, S. Jia and S. P. Williams, *Adv. Mater.*, 2010, **22**, 3839-3856.
2. B. C. Thompson and J. M. J. Fréchet, *Angew. Chem., Int. Ed.*, 2008, **47**, 58-77.
3. G. Dennler, M. C. Scharber and C. J. Brabec, *Adv. Mater.*, 2009, **21**, 1-16.
4. G. Dennler, S. Bereznev, D. Fichou, K. Holl, D. Ilic, R. Koeppe, M. Krebs, A. Labouret, C. Lungenschmied, A. Marchenko, D. Meissner, E. Mellikov, J. Méot, A. Meyer, T. Meyer, H. Neugebauer, A. Öpik, N. S. Sariciftci, S. Taillemite and T. Wöhrle, *Solar Energy*, 2007, **81**, 947-957.
5. D. Gendron and M. Leclerc, *Energy Environ. Sci.*, 2011, **4**, 1225-1237.
6. J. Chen and Y. Cao, *Acc. Chem. Res.*, 2009, **42**, 1709-1718.
7. Z. He, C. Zhong, S. Su, M. Xu, H. Wu and Y. Cao, *Nat. Photon.*, 2012, **6**, 591-595.
8. J. You, L. Dou, K. Yoshimura, T. Kato, K. Ohya, T. Moriarty, K. Emery, C.-C. Chen, J. Gao, G. Li and Y. Yang, *Nat. Commun.*, 2013, **4**, 1446.
9. C. J. Brabec, M. Heeney, I. McCulloch and J. Nelson, *Chem. Soc. Rev.*, 2011, **40**, 1185-1199.
10. W. Ma, C. Yang, X. Gong, K. Lee and A. J. Heeger, *Adv. Funct. Mater.*, 2005, **15**, 1617-1622.
11. G. Li, V. Shrotriya, J. Huang, Y. Yao, T. Moriarty, K. Emery and Y. Yang, *Nat. Mater.*, 2005, **4**, 864-868.
12. J. K. Lee, W. L. Ma, C. J. Brabec, J. Yuen, J. S. Moon, J. Y. Kim, K. Lee, G. C. Bazan and A. J. Heeger, *J. Am. Chem. Soc.*, 2008, **130**, 3619-3623.
13. J. Peet, J. Y. Kim, N. E. Coates, W. L. Ma, D. Moses, A. J. Heeger and G. C. Bazan, *Nat. Mater.*, 2007, **6**, 497-500.
14. T. Salim, L. H. Wong, B. Bräuer, R. Kukreja, Y. L. Foo, Z. Bao and Y. M. Lam, *J. Mater. Chem.*, 2011, **21**, 242-250.
15. S. Berson, R. De Bettignies, S. Bailly and S. Guillerez, *Adv. Funct. Mater.*, 2007, **17**, 1377-1384.
16. T. Salim, S. Sun, L. H. Wong, L. Xi, Y. L. Foo and Y. M. Lam, *J. Phys. Chem. C*, 2010, **114**, 9459-9468.
17. S. Sun, T. Salim, L. H. Wong, Y. L. Foo, F. Boey and Y. M. Lam, *J. Mater. Chem.*, 2011, **21**, 377-386.
18. H. Ma, H. L. Yip, F. Huang and A. K. Y. Jen, *Adv. Funct. Mater.*, 2010, **20**, 1371-1388.
19. R. Po, C. Carbonera, A. Bernardi and N. Camaioni, *Energy Environ. Sci.*, 2011, **4**, 285-310.

20. T. Salim, Z. Yin, S. Sun, X. Huang, H. Zhang and Y. M. Lam, *ACS Appl. Mater. Interfaces*, 2011, **3**, 1063-1067.
21. S. Berny, L. Tortech, M. Véber and D. Fichou, *ACS Applied Materials & Interfaces*, 2010, **2**, 3059-3068.
22. T. Ameri, G. Dennler, C. Lungenschmied and C. J. Brabec, *Energy Environ. Sci.*, 2009, **2**, 347-363.
23. S. Sista, Z. Hong, L.-M. Chen and Y. Yang, *Energy Environ. Sci.*, 2011, **4**, 1606-1620.
24. M. Koppe, H.-J. Egelhaaf, G. Dennler, M. C. Scharber, C. J. Brabec, P. Schilinsky and C. N. Hoth, *Adv. Funct. Mater.*, 2010, **20**, 338-346.
25. E. Lim, S. Lee and K. K. Lee, *Chem. Commun.*, 2011, **47**, 914-916.
26. C. S. Kim, L. L. Tinker, B. F. DiSalle, E. D. Gomez, S. Lee, S. Bernhard and Y.-L. Loo, *Adv. Mater.*, 2009, **21**, 3110-3115.
27. M. Campoy-Quiles, Y. Kanai, A. El-Basaty, H. Sakai and H. Murata, *Org. Electron.*, 2009, **10**, 1120-1132.
28. K. R. Graham, J. Mei, R. Stalder, J. W. Shim, H. Cheun, F. Steffy, F. So, B. Kippelen and J. R. Reynolds, *ACS Appl. Mater. Interfaces*, 2011, **3**, 1210-1215.
29. M. Shin, H. Kim, S. Nam, J. Park and Y. Kim, *Energy Environ. Sci.*, 2010, **3**, 1538-1543.
30. S. Berson, R. de Bettignies, S. Bailly, S. Guillerez and B. Jousselme, *Adv. Funct. Mater.*, 2007, **17**, 3363-3370.
31. Z. Xu, B. Hu and J. Howe, *J. Appl. Phys.*, 2008, **103**, 043909-043908.
32. B. P. Rand, C. Girotto, A. Mityashin, A. Hadipour, J. Genoe and P. Heremans, *Appl. Phys. Lett.*, 2009, **95**, 173304-173303.
33. Y. S. Kim, S. Baek, W. Lee, Y. Lee, S.-H. Han, C. Lee, Y.-S. Lee and S.-H. Lee, *J. Nanosci. Nanotechnol.*, 2009, **9**, 7167-7170.
34. Y. Shao and Y. Yang, *Adv. Mater.*, 2005, **17**, 2841-2844.
35. R. R. Lunt, N. C. Giebink, A. A. Belak, J. B. Benziger and S. R. Forrest, *J. Appl. Phys.*, 2009, **105**, 053711-053717.
36. I. Kim, H. M. Haverinen, Z. Wang, S. Madakuni, Y. Kim, J. Li and G. E. Jabbour, *Chem. Mater.*, 2009, **21**, 4256-4260.
37. G. L. Schulz and S. Holdcroft, *Chem. Mater.*, 2008, **20**, 5351-5355.
38. F. Guo, Y.-G. Kim, J. R. Reynolds and K. S. Schanze, *Chem. Commun.*, 2006, 1887-1889.
39. F. Guo, K. Ogawa, Y.-G. Kim, E. O. Danilov, F. N. Castellano, J. R. Reynolds and K. S. Schanze, *Phys. Chem. Chem. Phys.*, 2007, **9**, 2724-2734.
40. J. Mei, K. Ogawa, Y.-G. Kim, N. C. Heston, D. J. Arenas, Z. Nasrollahi, T. D. McCarley, D. B. Tanner, J. R. Reynolds and K. S. Schanze, *ACS Appl. Mater. Interfaces*, 2009, **1**, 150-161.
41. M. Arif, K. Yang, L. Li, P. Yu, S. Guha, S. Gangopadhyay, M. Forster and U. Scherf, *Appl. Phys. Lett.*, 2009, **94**, 063307-063303.
42. Y. Zhang, T. P. Basel, B. R. Gautam, X. Yang, D. J. Mascaro, F. Liu and Z. V. Vardeny, *Nat. Commun.*, 2012, **3**, 1043.
43. W. A. Luhman and R. J. Holmes, *Appl. Phys. Lett.*, 2009, **94**, 153304-153303.
44. Y. Li, R. Mastria, K. Li, A. Fiore, Y. Wang, R. Cingolani, L. Manna and G. Gigli, *Appl. Phys. Lett.*, 2009, **95**, 043101-043103.
45. S. T. Roberts, C. W. Schlenker, V. Barlier, R. E. McAnally, Y. Zhang, J. N. Mastron, M. E. Thompson and S. E. Bradforth, *J. Phys. Chem. Lett.*, 2010, **2**, 48-54.
46. B. P. Rand, S. Schols, D. Cheyns, H. Gommans, C. Girotto, J. Genoe, P. Heremans and J. Poortmans, *Org. Electron.*, 2009, **10**, 1015-1019.
47. A. Rao, P. C. Y. Chow, S. Gélinas, C. W. Schlenker, C.-Z. Li, H.-L. Yip, A. K.-Y. Jen, D. S. Ginger and R. H. Friend, *Nature*, 2013, **500**, 435-439.
48. E. Bittner, V. Lankevich, S. Gelinas, A. Rao, D. S. Ginger and R. Friend, *Phys. Chem. Chem. Phys.*, 2014, DOI: 10.1039/C4CP01776E.
49. C. Adachi, R. Kwong and S. R. Forrest, *Org. Electron.*, 2001, **2**, 37-43.
50. S. Cook, H. Ohkita, J. R. Durrant, Y. Kim, J. J. Benson-Smith, J. Nelson and D. D. C. Bradley, *Appl. Phys. Lett.*, 2006, **89**, 101128-101123.
51. F.-C. Chen, S.-C. Chang, G. He, S. Pyo, Y. Yang, M. Kurotaki and J. Kido, *Journal of Polymer Science Part B: Polymer Physics*, 2003, **41**, 2681-2690.
52. A. Köhler and D. Beljonne, *Adv. Funct. Mater.*, 2004, **14**, 11-18.
53. K. Sakurai, H. Tachibana, N. Shiga, C. Terakura, M. Matsumoto and Y. Tokura, *Phys. Rev. B*, 1997, **56**, 9552.
54. J. J. Benson-Smith, H. Ohkita, S. Cook, J. R. Durrant, D. D. C. Bradley and J. Nelson, *Dalton Trans.*, 2009, 10000-10005.
55. H. Wang, Q. Liao, H. Fu, Y. Zeng, Z. Jiang, J. Ma and J. Yao, *J. Mater. Chem.*, 2009, **19**, 89-96.
56. E. Verploegen, R. Mondal, C. J. Bettinger, S. Sok, M. F. Toney and Z. Bao, *Adv. Funct. Mater.*, 2010, **20**, 3519-3529.